



## Research paper

## Optimization of fluoride removal using calcined bauxite: Adsorption isotherms and kinetics

Vivian Kimambo<sup>a, bc, \*</sup>, Fanuel Josephat Ligata<sup>a, b</sup>, Julian Ijumulana<sup>a, b, d</sup>, Jyoti Prakash Maity<sup>e</sup>, Ron Jong<sup>f</sup>, Arslan Ahmad<sup>a, g</sup>, Rajabu Hamisi<sup>a</sup>, Joseph Mtamba<sup>b</sup>, Felix Mtalo<sup>b</sup>, Prosun Bhattacharya<sup>a, g</sup>

<sup>a</sup> KTH-Groundwater Arsenic Research Group, Department of Sustainable Development, Environmental Science and Engineering, KTH Royal Institute of Technology, 100 44, Stockholm, Sweden

<sup>b</sup> Department of Water Resources Engineering, University of Dar es Salaam, Dar es Salaam, Tanzania

<sup>c</sup> Department of Chemistry, College of Natural and Mathematical Sciences, University of Dodoma, Dodoma, Tanzania

<sup>d</sup> Department of Transportation and Geotechnical Engineering, College of Engineering and Technology, University of Dar Es Salaam, Dar es Salaam, Tanzania

<sup>e</sup> Environmental Science Laboratory, Department of Chemistry, School of Applied Sciences, KIIT Deemed to Be University, Bhubaneswar, Odisha, 751024, India

<sup>f</sup> KWR Water Research Institute, 3433 PE, Nieuwegein, the Netherlands

<sup>g</sup> SIBELCO Ankerpoort NV, Op de Bos 300, 6223 EP, Maastricht, the Netherlands

## ARTICLE INFO

## Keywords:

Geogenic contamination  
Fluorotic regions  
Drinking water  
Calcined natural bauxite  
Adsorption isotherms

## ABSTRACT

Geogenic contamination of groundwater due to elevated fluoride ( $F^-$ ) concentrations is a significant issue worldwide (including in Tanzania). The present study focussed to assess the adsorption capacity of thermally treated (calcined) bauxite to remove the  $F^-$  from contaminated water. Characterization of bauxite by X-ray fluorescence spectroscopy (XRF) revealed  $Al_2O_3$ ,  $Fe_2O_3$ , and  $SiO_2$  as the major oxides in both raw and calcined bauxite. The major mineral phase in the raw bauxite was gibbsite, which disappeared after calcination. The optimum calcination temperature, dosage and contact time for  $F^-$  removal by calcined bauxite were 400 °C, 40 g/L and 8 min, respectively. The experimental data revealed Freundlich isotherm as the best model to fit the  $F^-$  adsorption process with  $k_F$  and  $1/n$  being 0.1537 mg/g and 0.8607, respectively. The pseudo-second-order kinetic and intra-particle diffusion models explained well the  $F^-$  adsorption process with the rate constants of 115.43 g/mg min and 0.0025 mg/g min<sup>0.5</sup>, respectively. The values of  $\Delta G$ ,  $\Delta H$  and  $\Delta S$  indicate the  $F^-$  adsorption on bauxite surface indicated that the adsorption process was spontaneous, endothermic and structural changes occurred during the adsorption process. The  $F^-$  adsorption under optimum conditions lowered the pH and  $F^-$  concentration to WHO and Tanzania Bureau of Standards (TBS) standards.

## Nomenclature

## List of symbols

$C_0$	the initial fluoride concentration (mg/L)
$C_e$	the equilibrium fluoride concentration (mg/L)
$q_e$	the amount of fluoride adsorbed by 1 g of the adsorbent at equilibrium (mg/g)
$m$	the mass of adsorbent (g)
$V$	the volume of the $F^-$ solution (L)
$C_t$	the fluoride concentration at any time $t$ (mg/

$L$ )	
$q_t$	the amount of fluoride adsorbed on the surface of the adsorbent at any time $t$ (mg/g)
$\Delta G$	the Gibbs free energy change for the reaction (kJ/mol)
$\Delta S$	the entropy change for the reaction (kJ/mol K)
$\Delta H$	the enthalpy change for the reaction (kJ/mol)
$R$	the universal gas constant (8.314 J/mol K)
$T$	the temperature (K)
$K_c$	the adsorption equilibrium constant
$k_F$	the measure of adsorption capacity

\* Corresponding author. Teknikringen 10B, 100 44, Stockholm, Sweden.  
E-mail address: [kimambo@kth.se](mailto:kimambo@kth.se) (V. Kimambo).

<https://doi.org/10.1016/j.gsd.2023.100922>

Received 24 November 2022; Received in revised form 27 January 2023; Accepted 1 February 2023  
2352-801/© 20XX

**Table 1**

The countries with largest bauxite reserves (Hache et al., 2021; USGS 2020, 2021).

Country	Reserves of bauxite (thousand metric tons)	Percentage (%)
Guinea	7,400,000	24.92
Australia	5,100,000	17.17
Vietnam	3,700,000	12.46
Brazil	2,700,000	9.09
Jamaica	2,000,000	6.73
Indonesia	1,200,000	4.04
China	1,000,000	3.37
India	660,000	2.22
Russia	500,000	1.68
Saudi Arabia	190,000	0.64
Malaysia	170,000	0.57
Kazakhstan	160,000	0.54
Other countries	4,920,000	16.57
<b>Total</b>	<b>29,700,000</b>	<b>100</b>

$1/n$	the adsorption intensity
$b$	the Langmuir isotherm constant that relates to the energy of adsorption (L/mg)
$Q^o$	the amount of adsorbate at complete monolayer coverage (mg/g)
$R_L$	the Langmuir equilibrium factor
$t$	the time (min)
$k_{ad}$	the equilibrium rate constant for pseudo-first-order adsorption ( $\text{min}^{-1}$ )
$h$	the initial adsorption rate (mg/g min)
$k_p$	the particle rate constant ( $\text{min}^{-1}$ )
$k_{int}$	the intra-particle rate constant (mg/g $\text{min}^{0.5}$ )
$C$	the thickness of the boundary layer

## 1. Introduction

Fluoride intake in humans is essential for the formation and maintenance of healthy bones and teeth as long as it is within the WHO-acceptable limits (0.5–1.5 mg/L) (Kimambo et al., 2019; Maity et al., 2021). However, consumption of water with  $F^-$  above 1.5 mg/L can cause skeletal and dental fluorosis (Zhao et al., 2015). Surface water in

several parts of the world does not meet the quality requirements of different sectors, such as domestic, agricultural, and industrial sectors (Ahmad and Bhattacharya 2021; Bhattacharya and Bundschuh 2015). Therefore, groundwater serves as the major source of global freshwater (Bhattacharya and Bundschuh 2015; Coomar and Mukherjee 2021; Mukherjee et al., 2021). High concentrations of  $F^-$  have been reported in more than 35 countries of the world, exposing approximately 200 million people at the risk of fluorosis (Ayoob et al., 2008; Ijumulana et al., 2021, 2022). In northern parts of Tanzania, the  $F^-$  concentrations in groundwater have been observed above 10 mg/L (including Tanga, Arusha, Manyara, and Kilimanjaro regions). These regions lack alternative sources of drinking water (Ijumulana et al., 2021). This situation calls for attention to mitigate the problem by lowering  $F^-$  concentration below the maximum allowable concentration (Ndé-Tchoupé et al., 2015).

Several defluoridation techniques have been discussed in the literature, e.g. nano-filtration, adsorption, ion-exchange, coagulation, reverse osmosis, and electrochemical method (Maity et al., 2018). Each of these techniques has its strength and limitations. For example, ion exchange, coagulation, and electrochemical membrane methods require high installation and maintenance costs (Habuda-Stanić et al., 2014; Sivarajasekar et al., 2017). On the other hand, adsorption techniques require relatively modest investment and maintenance due to their simple design and availability of a wide range of materials that can be used as adsorbents (Bhatnagar et al., 2011). However, the applicability of some adsorbents is limited due to their low  $F^-$  removal capacity. Typically, the selection of adsorbent materials depends on the removal capacity, capital investment and running cost, local availability of materials, user preference, and acceptance by the community (Kimambo et al., 2019).

Bauxite is a naturally abundant mineral. The current estimation of global bauxite resources range between 55 and 75 billion tons (USGS 2021). Bauxites are divided into two main categories which are lateritic and karst bauxites. The main producers of lateritic bauxite are countries such as Guinea, India, Australia, North and South America while most of karst bauxite is produced by countries such as Jamaica, Greece, France, China, Russia, and Kazakhstan (Hache et al., 2021). The countries with largest bauxite reserves are shown in Table 1. Bauxite contains aluminium oxide, iron oxide, silica, and titanium oxides in variable amounts. The composition of different bauxites differs as a result of differences in the production and formation process (Alhassan et al., 2020).

**Table 2**

The fluoride adsorption capacity of bauxite under different adsorption conditions.

Adsorbent	Type of water	Initial $F^-$ Concentration (mg/L)	Particle size (mm)	Adsorbent dose (g/L)	Contact time (min)	pH	Temperature ( $^{\circ}C$ )	Shaking speed (rpm)	Adsorption capacity (mg/g)	References
Raw bauxite	RW	5	0.8–1.12		10,560	7	20	100	0.129	(Salifu et al., 2016)
Granular aluminum-coated bauxite	RW	5	0.8–1.12		10,560	7	20	100	0.335	(Salifu et al., 2016)
Granular aluminum-coated bauxite preheated at 500 $^{\circ}C$	RW	5	0.8–1.12		10,560	7	20	100	0.426	(Salifu et al., 2016)
Bauxite calcined at 200 $^{\circ}C$	SW	6	0.25	15	90	7	25–27		0.31	(Malakootian et al., 2015)
Bauxite calcined at 200 $^{\circ}C$	DW	2.46	0.25	15	90	7	25–27		0.087	(Malakootian et al., 2015)
Raw bauxite	SW	12	0.1	2	120	5–7	30	Not specified	2.4	Sujana and Anand (2011)
Bauxite calcined at 200 $^{\circ}C$	GW	12.62	0.5 – <1.0	1	180	8.72		125	1.05	(Thole et al., 2012a)

RW = Raw water.

SW = Synthetic water.

DW = Drinking water.

GW = Groundwater.

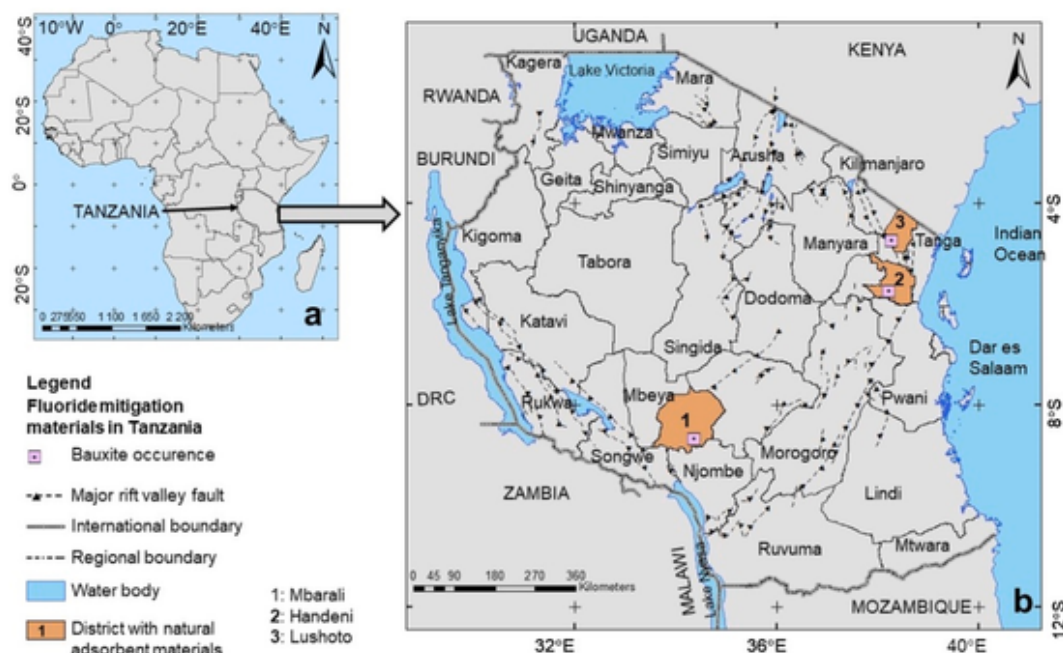


Fig. 1. Map showing the (a) location of Tanzania in Africa continent, (b) districts with bauxite mines in Tanzania.

Table 3

Percentages of oxides present in raw and bauxite calcined at 400 °C measured by using XRF.

Oxide	Raw bauxite	Bauxite calcined at 400 °C
$Al_2O_3$	57.67	66.98
$Fe_2O_3$	7.39	7.48
$SiO_2$	5.79	6.47
$TiO_2$	0.86	0.85
$CaO$	0.28	0.65
$P_2O_5$	0.17	0.14
$SO_3$	0.17	0.19
$V_2O_5$	0.07	<0.01
$Na_2O$	<0.01	<0.01
$MgO$	<0.01	<0.01
$K_2O$	<0.01	<0.01
$ZrO_2$	<0.01	<0.01
$NiO$	<0.01	<0.01
$Cr_2O_3$	<0.01	<0.01
$SrO$	<0.01	<0.01
$Cl$	<0.01	<0.01
LOI	27.59	17.24

Although raw bauxite can be used as an adsorbent for  $F^-$  removal from water, it contains impurities that can interfere with the adsorption and may leach unwanted ions into the treated water (Alhassan et al., 2020; Sajidu et al., 2012). The bauxite can be modified in order to improve its adsorption efficiency, ability to regenerate adsorbent, and the pH range in which it can adsorb  $F^-$  ions. The modification of adsorbent can change its surface chemistry and/or functional properties. Furthermore, the bauxite can be modified by metal impregnation, heating, acidifying, and crushing (Alhassan et al., 2020). The impregnation using metals e.g.,  $Al^{3+}$  increases the content of the gibbsite compared to hematite which increases  $F^-$  removal efficiency. Gibbsite being an aluminum-based oxide that possesses higher defluoridation capabilities than hematite which is an iron-based oxide (Salifu et al., 2016). Heating causes dehydroxylation which increases the surface area for binding (Ndé-Tchoupé et al., 2015) and lowers the time to reach equilibrium (Alhassan et al., 2020). Crushing increases the  $F^-$  removal capacity by increasing the surface area for binding (Alhassan et al., 2020). The  $F^-$  adsorption capacity of any adsorbent can be affected by several factors

(Kimambo et al., 2019). The adsorption capacity for  $F^-$  removal using bauxite at different experimental conditions is given in Table 2.

In Tanzania, large bauxite deposits are observed in Mbeya and Tanga regions. The total estimate of bauxite reserves in Kidundai-Magamba and Mabughai-Mlomboza bauxite deposits in the Tanga region is about 37 million tons (Mutakyahwa et al., 2003). Few studies on the application of bauxite from Tanzania for the defluoridation of water have been carried out (Thole et al., 2012a, 2012b, 2013). However, only few parameters which affect the  $F^-$  removal from water were tested. The current study aims to investigate the usability of bauxite from Tanzania and the factors which can affect its  $F^-$  removal capacity. The systematic batch experiment was performed and compared with modeling to better understand the removal of  $F^-$  by Tanzanian bauxite. The outcome this investigation intends to provide an effective and low-cost method for  $F^-$  removal from water.

## 2. Materials and methods

### 2.1. Geographical origins of the adsorbent and water samples

The bauxite used in this study was obtained from bauxite mine located in Lushoto District in Tanga Region, northeastern Tanzania. Fig. 1 shows the sampling location for the studied bauxite and other districts with bauxite mines in Tanzania.

The water sample used in this study was obtained from a natural spring (Supplementary Figure SF1) in the Arusha region, which is one of the largest regional  $F^-$  hotspots in northern Tanzania (Ijumulana et al., 2020). Water from this spring is used by the community as a drinking water source. According to the national population census of 2012, approximately 25% of the Northern Development Zone (NDZ) population lives in the Arusha region where only 30% of the groundwater sources are safe in terms of  $F^-$  levels for drinking purposes. This percentage is not adequate to accommodate the large population forcing most of the communities to depend on  $F^-$  contaminated water. As a consequence, the majority of community members in this region are prone to dental, skeletal, and crippling fluorosis (Ijumulana et al., 2021).

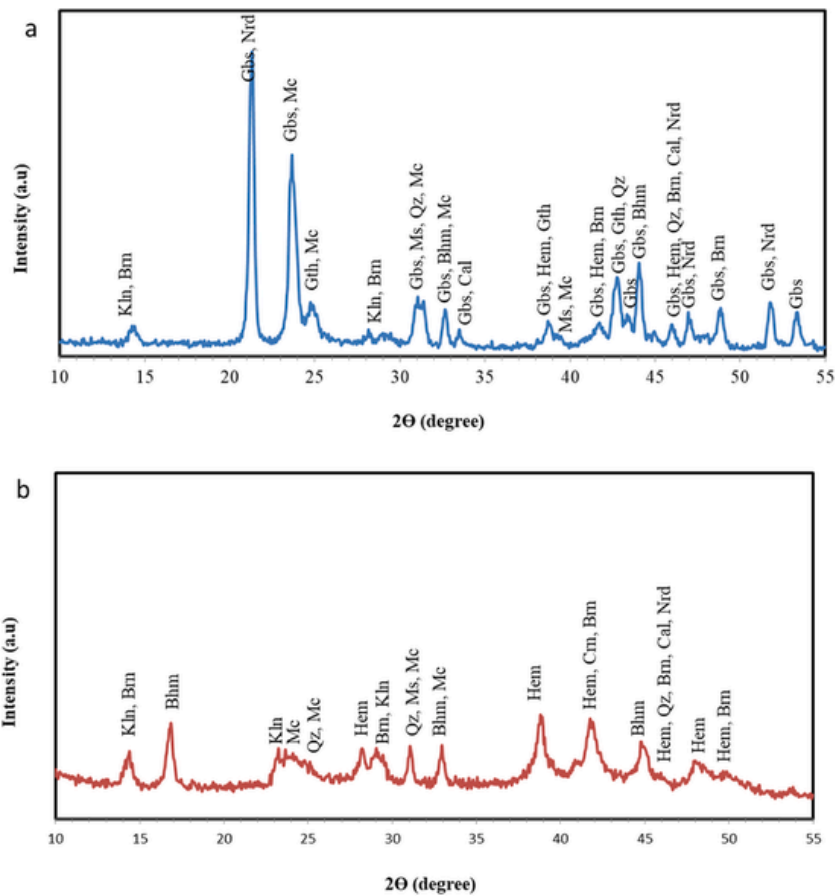


**Fig. 2.** XRD pattern for (a) raw bauxite (b) bauxite calcined at 400 °C  
Abbreviations: Bhm: boehmite ( $Al_2O_3 \cdot H_2O$ ); Brn: birnessite ( $Na_{0.3}Ca_{0.1}K_{0.1}Mn^{4+}Mn^{3+}O_{4.1.5}(H_2O)$ ); Cal: calcite ( $CaCO_3$ ); Crn: corundum ( $Al_2O_3$ ); Gbs: gibbsite ( $Al_2O_3 \cdot 3H_2O$ ); Gth: goethite ( $\alpha-FeO(OH)$ ); Hem: hematite ( $Fe_2O_3$ ); Kln: kaolinite ( $Al_2Si_2O_5(OH)_4$ ); Mc: microcline ( $KAlSi_3O_8$ ); Ms: muscovite ( $KAl_2(AlSi_3O_{10})$ ); Nrd: nordstrandite ( $Al(OH)_3$ ); Qz: quartz ( $SiO_2$ ).

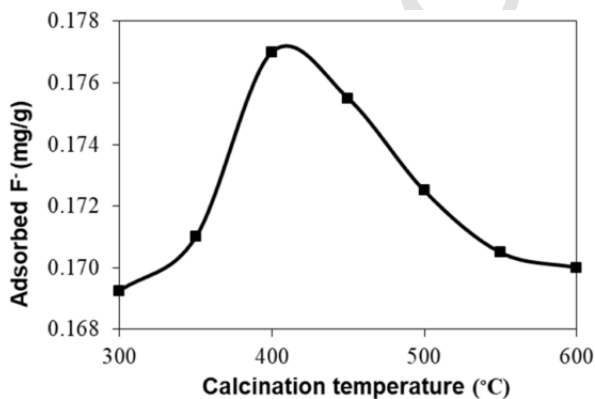


**Fig. 3.** Effect of calcination temperature on  $F^-$  adsorption on calcined bauxite which shows the loading capacity decrease after 400 °C due to sintering of materials and blockage of available pore space.

## 2.2. Preparations and characterization of adsorbent material

The Bauxite sample was ground and sieved until all the particles had a diameter of  $<0.075$  mm. The mineral phase composition was determined by BTX II X-ray Diffraction Analyzer (inXitu Inc, United States). The measurement was done using Co  $K\alpha_1$  over a range of 5–55° radiation at a wavelength of 1.78897 Å.

The chemical composition of bauxite material was determined by using an ARL OPTIM'X XRF spectrometer (Thermo Fisher Scientific Inc, Sweden).

## 2.3. Water sampling and analysis

A total of 60 L of water sample was collected from the spring and packed in three 20 L polyethylene cans. The GPS receiver Mobile Mapper 20 was used to record the location of the sampling site. The sampling procedures were followed during water sampling (EPA 2017). The samples were then transported to the Water Quality Laboratory of the University and Dar es Salaam and stored at 14 °C. Before the solution was mixed with the adsorbent, the pH and  $F^-$  concentrations were measured by using Hach® potable water quality multimeter (HQ40D). The pH calibration standards (4, 7, and 10) and ion concentration calibration standard solution of  $F^-$  (1, 5, and 10 mg/L) were usually applied (accuracy  $\pm 0.5\%$ ). The concentration of anions ( $Cl^-$ ,  $NO_3^-$ ,  $SO_4^{2-}$ ,  $HCO_3^-$ ) were determined by using Dionex DX-120 Ion Chromatography (IC). The concentration of cations ( $Al^{3+}$ ,  $As^{3+}$ ,  $Ba^{2+}$ ,  $Ca^{2+}$ ,  $Cd^{2+}$ ,  $Cr^{3+}$ ,  $Cu^{2+}$ ,  $Fe^{2+}$ ,  $Na^+$ ,  $Ni^{2+}$ ,  $Pb^{2+}$ ,  $Se^{2+}$ ,  $V^{5+}$ ,  $Zn^{2+}$ ,  $B^{3+}$ ) were analyzed by using Inductively Coupled Plasma Optical Emission Spectroscopy (ICP-OES). The speciation of inorganic ions and complexes in water samples before and after defluoridation were done by using Visual MINTEQ 3.1.

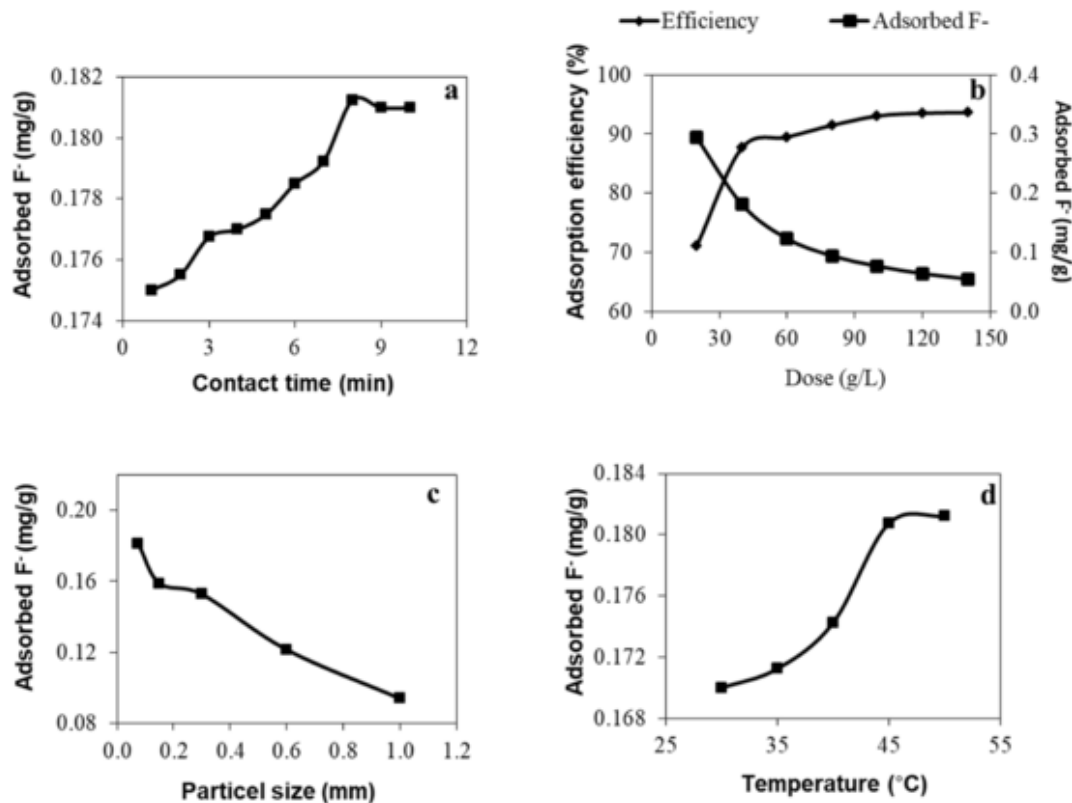


Fig. 4. Effect of (a) contact time (b) adsorbent dose (c) particle size and (d) temperature on fluoride removal by calcined bauxite.

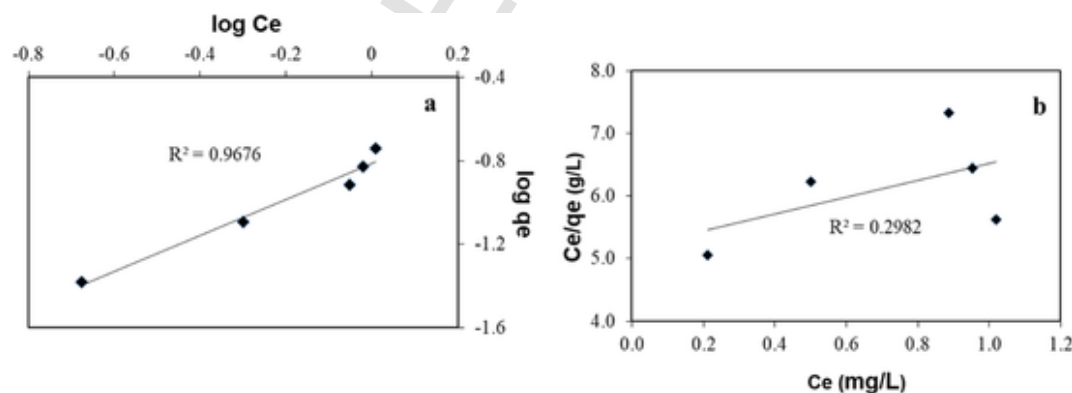


Fig. 5. Adsorption isotherms plot (a) Freundlich and (b) Langmuir for fluoride removal by calcined bauxite (adsorbent dose 40 g/L, shaking speed 200 rpm and temperature 30 °C).

#### 2.4. Batch experiments

Bauxite with 0.075 mm diameter was calcined in a Muffle furnace LE 1/11 (Nabertherm, Germany) at temperatures between 300 and 600 °C for 2 h. The batch experiments were designed to examine the effect of calcination temperature using 50 mL of 8.27 mg L<sup>-1</sup> F<sup>-</sup> raw water in conical flask, mixed with 2 g of bauxite with a shaker speed of 200 rpm for 4 min at 30 °C. After 4 min, the pH and F<sup>-</sup> concentration in remaining solution was measured. The calcination temperature which gave the highest adsorption capacity was used in subsequent experiments performed at different conditions i.e. contact time (1–10 min), adsorbent dose (20–140 g/L), particle size (0.075–1.0 mm) and temperature (30–50 °C) in order to determine the optimum conditions for the adsorption. The anions and cations in the water sample treated at optimum condition and were analyzed by using Dionex DX-120 Ion

Chromatography (IC) and Inductively Coupled Plasma Optical Emission Spectroscopy (ICP-OES), respectively.

The percent F<sup>-</sup> removal from aqueous media was calculated using Eq. (1) (Izuagie et al., 2015):

$$\% F^{-}\text{-removal} = \left( \frac{C_o - C_e}{C_o} \right) \times 100 \quad (1)$$

The amount of F<sup>-</sup> adsorbed by 1 g of the adsorbent at equilibrium (mg/g) was calculated using Eq. (2) (Maiti et al., 2011):

$$q_e = \frac{(C_o - C_e)}{m} \times V \quad (2)$$

The amount of adsorption at time t,  $q_t$  (mg/g) was calculated by Eq. (3) (Zhao et al., 2015):

**Table 4**  
Isotherm parameters for the removal of F<sup>-</sup> by calcined bauxite at 400 °C.

Model	Parameters	R <sup>2</sup>
Freundlich	$k_F = 0.154$ mg/g $1/n = 0.861$	0.968
Langmuir	$Q^o = 0.742$ mg/g $b = 0.261$ L/mg $R_L = 0.317$	0.298

$$q_t = \frac{(C_o - C_t)}{m} \times V \quad (3)$$

## 2.5. Adsorption isotherms

The two major adsorption models i.e. Freundlich and Langmuir adsorption isotherms were used to determine the mechanism and maximum adsorption capacity for F<sup>-</sup> adsorption on bauxite surface.

### 2.5.1. Freundlich isotherm

Freundlich isotherm model uses to describe the behaviour between adsorbate and adsorbent (Maity et al., 2018). Freundlich adsorption isotherm assumes multilayer adsorption on the heterogeneous surface (Sujana and Anand 2011) and the maximum adsorption occurs when the adsorbent surface is covered by adsorbate is given by Eq. (4):

$$\log q_e = \log k_F + \frac{1}{n} \log C_e \quad (4)$$

The values of  $k_F$  and  $1/n$  are calculated from the intercept and slope of the plot of  $\log q_e$  against  $\log C_e$  (Chen et al., 2010). The value of  $1/n$  between 0 and 1 indicates the adsorption process was favourable (Gogoi and Dutta 2015).

### 2.5.2. Langmuir isotherm

Langmuir isotherm model assumes monolayer adsorption on a homogeneous surface and there is no interaction between adsorbate molecules on adjacent sites. This means the adsorption capacity is the maxi-

mum (Maity et al., 2018). Langmuir equation which is purely empirical is given by Eq. (5):

$$\frac{C_e}{q_e} = \frac{1}{Q^o b} + \frac{C_e}{Q^o} \quad (5)$$

The slope and intercept of the graph of  $\frac{C_e}{q_e}$  against  $C_e$  give the value of  $Q^o$  and  $b$  (Meenakshi and Viswanathan 2007).

In order to find the practicability of the isotherm, the Langmuir isotherm was expressed in terms of the equilibrium factor ( $R_L$ ) by using Eq. (6)

$$R_L = \frac{1}{1 + bC_o} \quad (6)$$

The  $R_L$  value between 0 and 1 indicates the adsorption is favourable (Masindi et al., 2015).

## 2.6. Adsorption kinetics

Adsorption kinetics is one of the significant features of adsorbents which gives the awareness on the type and rate of adsorption (Haddad et al., 2019). The two major types of kinetics models which are the reaction and diffusion-based models were employed to study the kinetics of the adsorption process (Viswanathan et al., 2009, 2010).

### 2.6.1. Reaction based models

The reaction-based model is used to determine the rate of reaction (kinetic adsorption constant) for F<sup>-</sup> adsorption on calcined bauxite surface which is important in drawing valid conclusions and performing accurate modeling (Hosseini-bandegharai and Chao 2017).

The reaction-based models were used to study the adsorption of solutes from a liquid solution. The pseudo-first-order means the rate of reaction is proportional to the concentration of only one reactant (Maity et al., 2018). The pseudo-first-order kinetic model is given by Eq. (7):

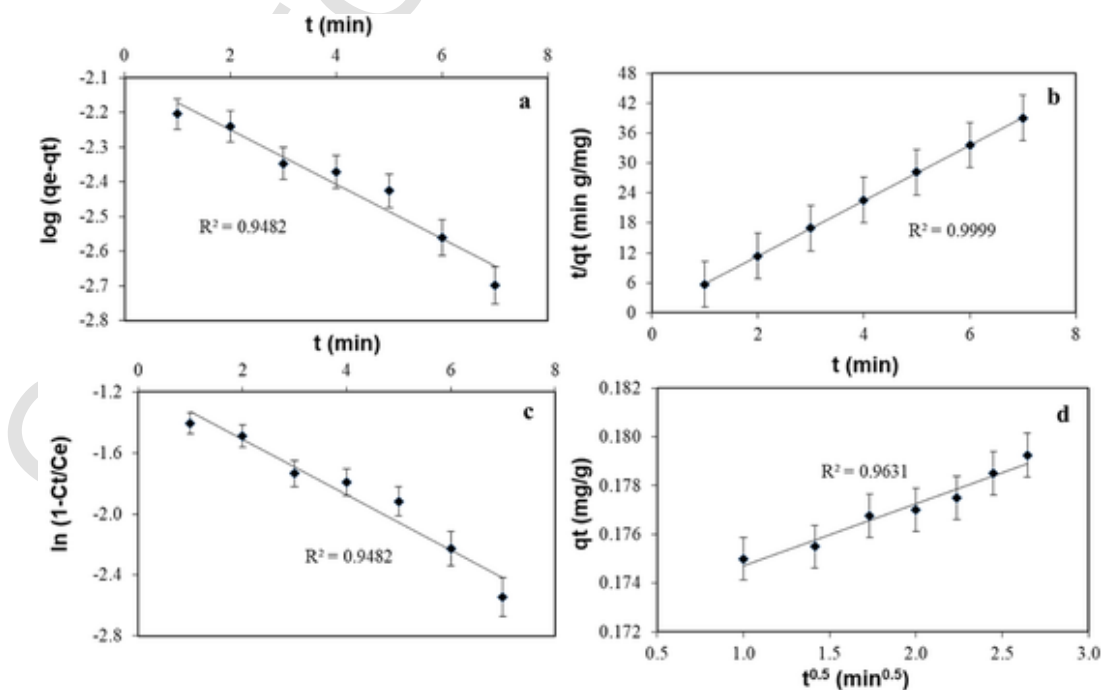


**Fig. 6.** Adsorption kinetics (a) pseudo-first-order, (b) pseudo-second-order, (c) particle diffusion controlled adsorption and (d) intra-particle diffusion controlled adsorption for fluoride removal by calcined bauxite (adsorbent dose 40 g/L, temperature 30 °C and shaking speed 200 rpm).

**Table 5**  
Thermodynamic parameters for F<sup>-</sup> adsorption on bauxite calcined at 400 °C.

$\Delta H$ (kJ/mol)	$\Delta S$ (kJ/mol K)	$\Delta G$ (kJ/mol)				
		303 K	308 K	313 K	318 K	323 K
19.892	0.078	-3.75	-4.14	-4.53	-4.92	-5.31

$$\log(q_e - q_t) = \log q_e - \frac{k_{ad}}{2.303} t \quad (7)$$

The value of  $k_{ad}$  was obtained from the slope of the graph of  $\log(q_e - q_t)$  against  $t$  (Viswanathan and Meenakshi 2008a, 2009).

The pseudo-second-order means the rate of reaction is proportional to the square of reactant concentrations (Maity et al., 2018). The linear pseudo-second-order is given by Eq. (8):

$$\frac{t}{q_t} = \frac{1}{h} + \frac{t}{q_e} \quad (8)$$

The values of  $q_e$  and  $h$  are obtained from the slope and intercept of the plot  $\frac{t}{q_t}$  against  $t$ . The pseudo-second-order rate constant  $k$  (g/mg min) is given by  $k = \text{slope}^2 / \text{intercept}$  (Suneetha et al., 2014; Viswanathan et al., 2010).

### 2.6.2. Diffusion-based models

In a solid-liquid adsorption process, the solute transfer is usually controlled by either particle or intra-particle diffusion. The contribution of diffusion on the rate of F<sup>-</sup> adsorption on calcined bauxite surface was studied by using particle and intra-particle diffusion models (Hosseini-bandegharai and Chao 2017).

The likelihood of the particle diffusion resistance affecting the adsorption behaviour was investigated using the particle diffusion kinetic model given by Eq. (9):

$$\ln\left(1 - \frac{C_t}{C_e}\right) = -k_p t \quad (9)$$

The graph of  $\ln\left(1 - \frac{C_t}{C_e}\right)$  against  $t$  gives the straight line with the value of  $k_p$  as the slope (Sundaram et al., 2008; Viswanathan and Meenakshi 2008b).

The intra-particle diffusion kinetic model was employed to study the contribution of intra-particle diffusion on the adsorption behaviour using Eq. (10):

$$q_t = k_{int} t^{\frac{1}{2}} + C \quad (10)$$

The plot of  $q_t$  against  $t^{\frac{1}{2}}$  gives the value of  $k_{int}$  as a slope (Haddad et al., 2019).

### 2.7. Thermodynamic parameters of adsorption

The thermodynamic properties were studied by changing the temperature in the thermostat-controlled shaker from 30 to 50 °C (303–323 K). The thermodynamic parameters  $\Delta G$ ,  $\Delta S$  and  $\Delta H$  associated with the adsorption were calculated in order to determine the nature of F<sup>-</sup> adsorption process.

The  $\Delta G$  of the adsorption process is calculated from Eq. (11) (Sujana and Anand 2011):

$$\Delta G = -RT \ln K_c \quad (11)$$

The  $\Delta G$  was also expressed in terms of  $\Delta H$  and  $\Delta S$  by using Eq. (12):

$$\Delta G = \Delta H - T \Delta S \quad (12)$$

The value of  $\Delta G$  for the reaction is used to predict whether the reaction can take place spontaneously ( $\Delta G < 0$ ) or the application the energy is required in order to promote the reaction ( $\Delta G > 0$ ).

The adsorption distribution constant was expressed in terms of  $\Delta H$  and  $\Delta S$  as a function of temperature ( $T$ ) using Eq. (13):

$$\ln K_c = \frac{-\Delta H}{RT} + \frac{\Delta S}{R} \quad (13)$$

The values of  $\Delta H$  and  $\Delta S$  were calculated from the slope and intercept of the plot of  $\ln K_c$  against  $\frac{1}{T}$ . The negative and positive  $\Delta H$  indicates exothermic and endothermic reaction, respectively. The value of  $\Delta S > 0$  means the reaction irreversible and stable (Viswanathan and Meenakshi 2008a).

### 2.8. Regeneration of bauxite

The used bauxite was regenerated by shaking them in 0.015 mol/L NaOH solution for 2 h and filtered (Das et al., 2005). The filtrate was then washed using distilled water in order to remove excessive NaOH from the adsorbent. The material was dried for 24 h at room temperature before oven dried at 105 °C for 3 h. The regenerated bauxite was used for F<sup>-</sup> removal under optimum conditions.

## 3. Results and discussion

### 3.1. Characterization of the adsorbent materials

#### 3.1.1. Chemical composition

The data shows that the  $Al_2O_3$ ,  $Fe_2O_3$  and  $SiO_2$  were the major oxides in untreated and calcined bauxite (Table 3) however, the percentages of the major oxides differ from that reported in another study. A study by Thole et al. (2013) reported 30.33% ( $Al_2O_3$ ), 14.3% ( $Fe_2O_3$ ) and 15.0% ( $SiO_2$ ).

#### 3.1.2. Mineralogical composition

The XRD data indicate the gibbsite ( $Al_2O_3 \cdot 3H_2O$ ) is the major constituent of raw bauxite (Fig. 2a). The presence of the gibbsite is indicated by characteristic peaks at 'd' values of 4.81, 2.45, and 1.99, etc. The other minerals which are present in raw bauxite are presented in Supplementary Table ST1. The results were in positive agreement with those reported by Mutakyahwa et al. (2003).

On calcination at 400 °C gibbsite peaks disappeared (Fig. 2b) because of the loss of water molecules to form boehmite ( $Al_2O_3 \cdot H_2O$ ) (Eq. (14)) and corundum ( $Al_2O_3$ ) (Eq. (15)) (Supplementary Table ST2). Loss of water can also be the reason for the disappearance of goethite peaks and the increase in the amount of hematite ( $Fe_2O_3$ ) in calcined bauxite (Eq. (16)). Similar results were observed in the study by Das et al. (2005).



### 3.2. Raw water composition

The pH and ionic status of the water are shown in Supplementary Table ST3. The concentrations of F<sup>-</sup>, and Ca<sup>2+</sup> as well as pH, were observed above the WHO limit (WHO 2011) and TBS standards (TBS 2009) while that of Cl<sup>-</sup>, NO<sub>3</sub><sup>-</sup> and SO<sub>4</sub><sup>2-</sup> were below the standards.

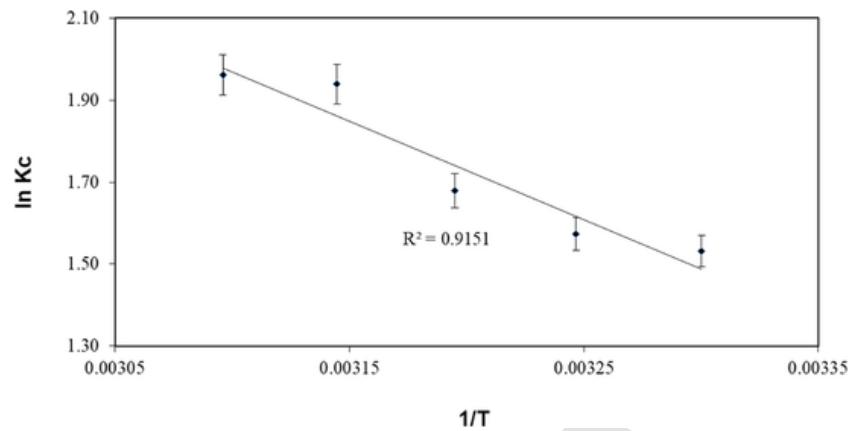


Fig. 7. Fluoride removal by calcined bauxite: Fitting curve between  $\ln K_c$  against  $1/T$  (adsorbent dose 40 g/L and shaking speed 200 rpm).

### 3.3. Fluoride removal experiments

#### 3.3.1. Impact of calcination temperature

The calcined bauxite showed different adsorption loading at different temperatures. Initially, the adsorption loading increased with the increase in calcination temperature from 200 to 400 °C (Fig. 3). This occurred because gibbsite undergoes dehydroxylation processes to form boehmite (300 °C) followed by  $Al_2O_3$  (above 300 °C) which increased the surface area of bauxite, hence increase the uptake loading (Das et al., 2005). After 400 °C the adsorption loading started to decrease due to the sintering of materials and blockage of available pore space. Das et al. (2005) reported a similar  $F^-$  adsorption trend. The calcination temperature which gave the highest adsorption loading (400 °C) was fixed as the calcination temperature for the subsequent experiment.

#### 3.3.2. Effect of contact time

Initially, the adsorption loading increased with an increase in time (Fig. 4a). The increase was caused by the fact that initially, the large number of active sites were vacant and the solute concentration gradients were high which favored high mass transfer on the surface of the adsorbent (Singh et al., 2018). After 8 min, the  $F^-$  removal capacity remained constant that indicating the adsorption has attained the equilibrium. Therefore, 8 min was fixed as the contact time for subsequent experiments. This indicates the reaction between bauxite and  $F^-$  proceeds at high speed.

#### 3.3.3. Effect of adsorbent dose

Initially, the adsorption efficiency increased with an increase in adsorbent dose as shown in Fig. 4b. This was caused by the increase in the number of active sites available for adsorption per unit weight of  $F^-$  treated (Singh et al., 2018). After the dose of 40 g/L, there were no significant increases in the adsorption efficiency. This is because of decrease in  $F^-$  to the available active sites ratio with an increase in the amount of the adsorbent (Fufa et al., 2014). On the other hand, the adsorption loading decreased with the increase in the adsorbent dose due to the overlapping of active sites as the amount of adsorbent increased per unit volume (Kumar et al., 2007; Rajkumar et al., 2019).

#### 3.3.4. Effect of particle size

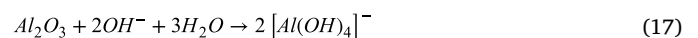
Fig. 4c shows the adsorption loading decreased with the increase in particle size. A smaller particle size increases the  $F^-$  adsorption uptake by increasing the availability of reactive surface areas on the adsorbent surface. These results are in accordance with Thole et al. (2012a) and Malakootian et al. (2017). The 0.075 mm was fixed as the particle size for the subsequent experiment.

#### 3.3.5. Temperature

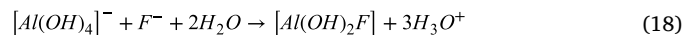
The adsorption was increased with the increase in temperature from 30 to 50 °C (Fig. 4d). This can be caused by the decrease in thickness of the outer surface of the bauxite which increased the rate of diffusion of  $F^-$  across the internal pores and external boundary layer of the calcined bauxite (Suneetha et al., 2014). Also the kinetic energy of  $F^-$  increases due to the increase in temperature which can be the reason for the increase in  $F^-$  uptake (Kundu et al., 2017). The increase of uptake with the increase in temperature indicated  $F^-$  adsorption on calcined bauxite is an endothermic reaction (Abe et al., 2004).

#### 3.4. Effect of adsorption on the quality of water

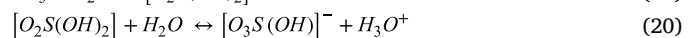
The results from Supplementary Table ST3 show the adsorption using calcined bauxite was able to lower the concentration of  $F^-$  and the pH of groundwater to the WHO and TBS standard levels. After the adsorption, the  $F^-$  concentration and the pH of water was lower from 8.27 to 1.02 mg/L and 9.38 to 6.74, respectively. Bauxite was able to lower the pH of water because it contains a large amount of  $Al_2O_3$  which is an amphoteric character. Being amphoteric,  $Al_2O_3$  has the ability to react as an acid in the basic water medium and lowers the pH by reducing the concentration of  $OH^-$  in water (Eq. (17)).



Then following the adsorption process whereby protons are released to the surrounding medium hence decrease of water pH further (Eq. (18)).



The presence of sulphite which is largely acidic can also cause decrease in pH. During dissolution sulphite from bauxite bind water molecules and discharge protons to the surrounding medium which cause the pH of water to decrease (Thole et al., 2013) (Eqs. (19) and (20))



After treatment the concentration of some ions i.e.  $Al^{3+}$  and  $B^{3+}$  increased in water, however, they were still within the allowed values. The concentration of  $Cr^{3+}$  and  $Ca^{2+}$  in water after treatment did not adhere to the upper WHO  $Cr^{3+}$  and  $Ca^{2+}$  limit.

#### 3.5. Adsorption isotherms

Freundlich isotherm model was found to be the best fitting model for the adsorption of  $F^-$  on the adsorbent since it gives a straight line

**Table 6**

Estimation and costing for the preparation of calcined bauxite per kg.

Sl. No.	Item	Unit Cost (Tsh)	Consumption	Price (Tsh)	Price (\$) (As on June 30, 2021)
1	Bauxite Collection	1315.60		1315.60	0.56
2	Grinder	292.74 per kWh	0.25 kWh for 0.5 h	36.59	0.02
3	Sieving	292.74 per kWh	0.25 kWh for 0.25 h	18.30	0.01
4	Calcining	292.74 per kWh	1.6 kWh for 2 h	936.77	0.40
	Net Cost			2307.26	0.98
	Other Overhead Cost (10% of Net Cost)			230.73	0.10
	<b>Total Cost</b>			<b>2537.99</b>	<b>1.08</b>

with the correlation coefficient close to unity (Fig. 5a and b). This indicates multilayer adsorption on the heterogeneous surface. The values  $1/n$  and  $R_L$  were found to be between 0 and 1 (Table 4) which shows that the adsorption process was favourable. These results were in agreement with Salifu et al., (2016), Atasoy et al. (2013) and Malakootian et al. (2014).

### 3.6. Adsorption kinetics

#### 3.6.1. Reaction-based models

The correlation coefficient ( $r$ ) in the pseudo-second-order model was higher than that of the pseudo-first-order model (Fig. 6a and b) which indicates the applicability of the pseudo-second-order model (Viswanathan and Meenakshi 2008a, 2008b). Pseudo-second-order also has larger adsorption loading at equilibrium (0.180 mg/g) compared to the pseudo-first order (0.008 mg/g). The rate constants for pseudo-first-order and pseudo-second-order were observed to be 0.181 min<sup>-1</sup> and 115.425 g/mg min, respectively. These results agreed with Malakootian et al. (Malakootian et al., 2014, 2015, 2017), Haddad et al. (2019) and Salifu et al. (2016).

#### 3.6.2. Diffusion-based models

The rate constants for particle and intra-particle diffusion models were found to be 0.1813 min<sup>-1</sup> and 0.0025 mg/g min<sup>0.5</sup>, respectively (Fig. 6c and d) The higher correlation coefficient ( $r$ ) values for intra-particle diffusion models which indicate that the F<sup>-</sup> diffusion on adsorbent follows intra-particle diffusion models. This observation for F<sup>-</sup> adsorption is consistent with the findings by Sujana and Anand (2011).

### 3.7. Thermodynamic parameters

The negative values of  $\Delta G$  (Table 5) obtained from Fig. 7 confirm the spontaneous nature of the adsorption process at all temperatures studied. The value of  $\Delta G$  became more negative with the increase in temperature that indicates the F<sup>-</sup> removal process is favored by the increase in temperature (Mourabet et al., 2011). The results obtained from this study concur with those reported in earlier studies (Sujana and Anand 2011; Salifu et al., 2016) where the spontaneous nature of F<sup>-</sup> adsorption occurred on bauxite surface.

The value of  $\Delta G$  being between 0 and -20 kJ/mol indicates the physisorption on the bauxite surface (Salifu et al., 2016). The  $\Delta G$  value of -5.44 kJ/mol was reported by Sujana and Anand (2011). The endothermic nature of F<sup>-</sup> adsorption on calcined bauxite is indicated by the value of  $\Delta H > 0$ . The positive value of  $\Delta S$  indicates good affinity of F<sup>-</sup> towards bauxite and the randomness at the solid/solution interface increased during the adsorption process (Maity et al., 2018; Mourabet et al., 2011).

### 3.8. Speciation of inorganic ions and complexes in water sample

The comparison between the concentration of Species present in water before and after defluoridation is shown in Supplementary Table ST4. The total concentrations of aluminofluoride (AlF<sub>x</sub>) complexes in treated water are very low (5.18E-07 mg/L) means that its consumption cannot lead to chronic kidney disease (CKD) (Wasana et al., 2015).

### 3.9. Regeneration of bauxite

After the regeneration, the F<sup>-</sup> adsorption efficiency of calcined bauxite decreased from 87.67 to 78.23%. The amount of F<sup>-</sup> remained in water when bauxite was regenerated was 1.8 mg/L which is slightly above the WHO standard (1.5 mg/L). The effectiveness F<sup>-</sup> removal ability decreased after regeneration due to the fact that several chemical reactions take place on the bauxite surface during adsorption which caused some pores to collapse (Li et al., 2020).

## 4. Cost analysis

The cost of adsorbent preparation is very important in order to determine the overall cost for large scale applicability and economic feasibility of the process. It is very difficult to select the adsorbent without cost estimation (Tirkey et al., 2018). In this study, low cost bauxite was proposed as the adsorbent for fluoride removal from water. Bauxite is locally available in several regions of Tanzania and around the world. The production cost of a unit of calcined bauxite depends on the collection and process cost which includes electricity consumption in the oven, crusher, sieve and muffle furnace, which was found to be 8334.58 TSh ( $\approx 3.55$  US\$ kg<sup>-1</sup> as on June 30, 2022) at laboratory scale (Table 6). The cost of electricity consumption can be reduced  $\approx 1.08$  US\$ kg<sup>-1</sup> by drying the bauxite in sunlight, but it will take more time to dry. This cost is low as compared to technologies using other adsorbents available in the market e.g. the production of activation carbon is 8.40 US\$ kg<sup>-1</sup> (Sharma et al., 2021).

## 5. Conclusion

Calcined bauxite offers a higher F<sup>-</sup> removal efficiency than the raw bauxite due to phase changes that occurred during calcination which also increased the surface area of the bauxite. The data from adsorption experiments fit well with the Freundlich isotherm which indicates multilayer adsorption. The adsorption kinetics model indicates F<sup>-</sup> adsorption on bauxite surface follows intra-particle diffusion and pseudo-second-order models. The negative  $\Delta G$ , positive  $\Delta H$  and positive  $\Delta S$  indicate the F<sup>-</sup> adsorption on the bauxite surface was spontaneous, endothermic, and structural changes which occurred during the adsorption process. The F<sup>-</sup> adsorption capacity was lower than that reported in other literature. This may be due to the higher pH which caused F<sup>-</sup> to compete with OH<sup>-</sup> for the sorption site on the bauxite surface. The effectiveness of adsorbent for F<sup>-</sup> removal is reduced after each regeneration. The concentrations of inorganic ions and complexes present in treated water indicate that it complies with the drinking water standard. The results obtained from this study revealed the potential usefulness of calcined bauxite for F<sup>-</sup> removal from water, however, the disposal the F<sup>-</sup> loaded calcined bauxite is still a problem. The overall cost-benefit analysis reveals that the cost of calcined bauxite for safe water production is low as compared to other available adsorbents.

### Declaration of competing interest

The authors declare the following financial interests/personal relationships which may be considered as potential competing interests: Prosun Bhattacharya & Felix Mtalto reports financial support was provided by Swedish International Development Cooperation Agency. Vi-

vian Kimambo reports a relationship with The University of Dodoma that includes:

## Data availability

Data will be made available on request.

## Acknowledgement

This work was supported by Swedish International Development Cooperation Agency (Sida) [Contribution number 51170072, 2015–2022]. The authors would like to acknowledge the Government Chemist Laboratory Agency (GCLA) for analysis of cations and anions in the water sample. The authors are also appreciative to the Department of Geology (University of Dar es Salaam) and African Minerals and Geosciences Centre for the analysis of mineral phase and chemical composition of bauxite samples, respectively.

## Appendix A. Supplementary data

Supplementary data to this article can be found online at <https://doi.org/10.1016/j.gsd.2023.100922>.

## References

- Abe, I., Iwasaki, S., Tokimoto, T., Kawasaki, N., Nakamura, T., Tanada, S., 2004. Adsorption of fluoride ions onto carbonaceous materials. *J. Colloid Interface Sci.* 275 (1), 35–39. <https://doi.org/10.1016/j.jcis.2003.12.031>.
- Ahmad, A., Bhattacharya, P., 2021. Global groundwater: source, scarcity, security and solutions. *Groundwater for Sustainable Development* 15 (June), 1–2. <https://doi.org/10.1016/j.gsd.2021.100605>.
- Alhassan, S.I., He, Y., Huang, L., Wu, B., Yan, L., Deng, H., Wang, H., 2020. A review on fluoride adsorption using modified bauxite: surface modification and sorption mechanisms perspectives. *J. Environ. Chem. Eng.* 8 (6), 104532. <https://doi.org/10.1016/j.jece.2020.104532>.
- Atasoy, A.D., Yesilnacar, M.I., Sahin, M.O., 2013. Removal of fluoride from contaminated ground water using raw and modified bauxite. *Bull. Environ. Contam. Toxicol.* 91 (5), 595–599. <https://doi.org/10.1007/s00128-013-1099-z>.
- Ayoob, S., Gupta, A.K., Bhat, V.T., 2008. A conceptual overview on sustainable technologies for the defluoridation of drinking water. *Crit. Rev. Environ. Sci. Technol.* <https://doi.org/10.1080/10643380701413310>.
- Bhatnagar, A., Kumar, E., Sillanpää, M., 2011. Fluoride removal from water by adsorption-A review. *Chem. Eng. J.* <https://doi.org/10.1016/j.ccej.2011.05.028>.
- Bhattacharya, P., Bundschuh, J., 2015. Groundwater for sustainable development – cross cutting the UN sustainable development goals – editorial. *Groundwater for Sustainable Development* 1, 155–157. <https://doi.org/10.1016/j.gsd.2016.04.004>.
- Chen, N., Zhang, Z., Feng, C., Sugiura, N., Li, M., Chen, R., 2010. Fluoride removal from water by granular ceramic adsorption. *J. Colloid Interface Sci.* 348 (2), 579–584. <https://doi.org/10.1016/j.jcis.2010.04.048>.
- Coomar, P., Mukherjee, A., 2021. Global Geogenic Groundwater Pollution. *Global Groundwater. INC.* <https://doi.org/10.1016/B978-0-12-818172-0.00014-1>.
- Das, N., Pattanaik, P., Das, R., 2005. Defluoridation of drinking water using activated titanium rich bauxite. *J. Colloid Interface Sci.* 292 (1), 1–10. <https://doi.org/10.1016/j.jcis.2005.06.045>.
- EPA, 2017. Sampling Guidance for Unknown Contaminants in Drinking Water, United States Environmental Protection Agency, pp. 1–60. Retrieved from. [https://www.oecd-ilibrary.org/environment/diffuse-pollution-degraded-waters\\_9789264269064-en](https://www.oecd-ilibrary.org/environment/diffuse-pollution-degraded-waters_9789264269064-en).
- Fufa, F., Alemayehu, E., Deboch, B., 2014. Defluoridation of Groundwater Using Gypsiferous Limestone, vol. 3. pp. 71–76. <https://doi.org/10.5455/jeos.201403140417432>.
- Gogoi, S., Dutta, R.K., 2015. Mechanism of fluoride removal by phosphoric acid-enhanced limestone: equilibrium and kinetics of fluoride sorption. *Desalination Water Treat.* 3994 (September), 1–14. <https://doi.org/10.1080/19443994.2015.1010592>.
- Habuda-Stanić, M., Ravančić, M., Flanagan, A., 2014. A review on adsorption of fluoride from aqueous solution. *Materials* 7 (9), 6317–6366. <https://doi.org/10.3390/ma7096317>.
- Hache, E., Barnet, C., Seck, G., 2021. Aluminium in the energy transition: what lies ahead for this indispensable metal of the modern world? *Metals in the Energy Transition* 6 (May).
- Haddad, A.Z., Pilgrim, C.D., Sawvel, A.M., Hohman, J.N., Gadgil, A.J., 2019. On the conversion of bauxite ores to highly activated alumina media for water remediation. *Journal of Advanced Sustainable System* 3 (7). <https://doi.org/10.1002/adu.201900005>.
- Hosseini-bandegharai, A., Chao, H., 2017. Mistakes and inconsistencies regarding adsorption of contaminants from aqueous solutions: a critical review. *Water Res.* 120 (May), 88–116. <https://doi.org/10.1016/j.watres.2017.04.014>.
- Ijumulana, J., Ligate, F., Bhattacharya, P., Mtalo, F., Chaosheng, Z., 2020. Spatial analysis and GIS mapping of regional hotspots and potential health risk of fluoride concentrations in groundwater of northern Tanzania. *Sci. Total Environ.* 735 (139584), 1–16. <https://doi.org/10.1016/j.scitotenv.2020.139584>.
- Ijumulana, J., Ligate, F., Irunde, R., Bhattacharya, P., Ahmad, A., Tomašek, I., Mtalo, F., 2022. Spatial Variability of the Sources and Distribution of Fluoride in Groundwater of the Sanya Alluvial Plain Aquifers in Northern Tanzania, vol. 810. *Science of the Total Environment.* <https://doi.org/10.1016/j.scitotenv.2021.152153>.
- Ijumulana, J., Ligate, F., Irunde, R., Bhattacharya, P., Prakash, J., Ahmad, A., Mtalo, F., 2021. Spatial uncertainties in fluoride levels and health risks in endemic fluorotic regions of northern Tanzania. *Groundwater for Sustainable Development* 14 (100618), 1–14. <https://doi.org/10.1016/j.gsd.2021.100618>.
- Izuagie, A.A., Gitari, W.M., Gumbo, J.R., 2015. Defluoridation of groundwater using diatomaceous earth: optimization of adsorption conditions, kinetics and leached metals risk assessment. *Desalination Water Treat.* 1–13. <https://doi.org/10.1080/19443994.2015.1083894>.
- Kimambo, V., Bhattacharya, P., Mtalo, F., Mtamba, J., Ahmad, A., 2019. Fluoride occurrence in groundwater systems at global scale and status of defluoridation – state of the art. *Groundwater for Sustainable Development* 9 (August 2018), 1–18. <https://doi.org/10.1016/j.gsd.2019.100223>.
- Kumar, S., Gupta, A., Yadav, J.P., 2007. Fluoride removal by mixtures of activated carbon prepared from Neem (*Azadirachta indica*) and Kikar (*Acacia arabica*) leaves. *Indian J. Chem. Technol.* 14, 355–361.
- Kundu, S., Chowdhury, I.H., Sinha, P.K., Naskar, M.K., 2017. Effect of organic acid-modified mesoporous alumina toward fluoride ions removal from water. *J. Chem. Eng. Data* 62 (7), 2067–2074. <https://doi.org/10.1021/acs.jced.7b00129>.
- Li, H., Liu, L., Cui, J., Cui, J., 2020. High-efficiency adsorption and regeneration of methylene blue and aniline onto activated carbon from waste edible fungus residue and its possible. *RSC Adv.* 10, 14262–14273. <https://doi.org/10.1039/d0ra01245a>.
- Maiti, A., Basu, J.K., De, S., 2011. Chemical treated laterite as promising fluoride adsorbent for aqueous system and kinetic modeling. *Desalination* 265 (1–3), 28–36. <https://doi.org/10.1016/j.desal.2010.07.026>.
- Maiti, J.P., Hsu, C.M., Lin, T.J., Lee, W.C., Bhattacharya, P., Bundschuh, J., Chen, C.Y., 2018. Removal of fluoride from water through bacterial-surfactin mediated novel hydroxyapatite nanoparticle and its efficiency assessment: adsorption isotherm, adsorption kinetic and adsorption Thermodynamics. *Environ. Nanotechnol. Monit. Manag.* 9, 18–28. <https://doi.org/10.1016/j.enmm.2017.11.001>.
- Maiti, J., Vithanage, M., Kumar, M., Ghosh, A., Mohan, D., Ahmad, A., 2021. Seven 21st century challenges of arsenic-fluoride contamination and remediation. *Groundwater for Sustainable Development* 12 (December 2020). <https://doi.org/10.1016/j.gsd.2020.100538>.
- Malakootian, M., Javdan, M., Iranmanesh, F., 2014. Fluoride removal from aqueous solutions using bauxite activated mines in yazd province (case study: kuhbanan water). *Journal of Community Health Research* 3 (2), 103–117.
- Malakootian, M., Javdan, M., Iranmanesh, F., 2015. Fluoride removal study from aqueous solutions using jajarm bauxite: case study on koohbanan water. *Fluoride* 48 (2), 113–122.
- Malakootian, M., Javdan, M., Iranmanesh, F., 2017. Use of bauxite from active Iranian mines for the removal of fluoride from drinking water. *Journal of Environmental Health Engineering and Management* 4 (4), 217–224. <https://doi.org/10.15171/EHEM.2017.30>.
- Masindi, V., Gitari, W.M., Ngulube, T., 2015. Kinetics and equilibrium studies for removal of fluoride from underground water using cryptocrystalline magnesite. *Journal of Water Reuse and Desalination* 5 (3), 282–292. <https://doi.org/10.2166/wrd.2015.080>.
- Meenakshi, S., Viswanathan, N., 2007. Identification of selective ion-exchange resin for fluoride sorption. *J. Colloid Interface Sci.* 308 (2), 438–450. <https://doi.org/10.1016/j.jcis.2006.12.032>.
- Mourabet, M., El Boujaady, H., El Rhilassi, A., Ramdane, H., Bennani-Ziatni, M., El Hamri, R., Taitai, A., 2011. Defluoridation of water using Brushite: equilibrium, kinetic and thermodynamic studies. *Desalination.* <https://doi.org/10.1016/j.desal.2011.05.068>.
- Mukherjee, A., Scanlon, B.R., Aureli, A., Langan, S., Guo, H., McKenzie, A., 2021. Global groundwater: from scarcity to security through sustainability and solutions. In: *Global Groundwater. INC.*, pp. 1–20. <https://doi.org/10.1016/B978-0-12-818172-0.00001-3>.
- Mutakyahwa, M.K.D., Ikingura, J.R., Mruma, A.H., 2003. Geology and geochemistry of bauxite deposits in Lushoto district, usambara mountains, Tanzania. *J. Afr. Earth Sci.* 36, 357–369. [https://doi.org/10.1016/S0899-5362\(03\)00042-3](https://doi.org/10.1016/S0899-5362(03)00042-3).
- Ndè-Tchoupé, A.I., Crane, R.A., Mwakabona, H.T., Noubactep, C., Njau, K.N., 2015. Technologies for decentralized fluoride removal: testing metallic iron-based filters. *Water (Switzerland)* 7 (12), 6750–6774. <https://doi.org/10.3390/w7126657>.
- Rajkumar, S., Murugesu, S., Sivasankar, V., Darchen, A., Msagati, T.A.M., Chaabane, T., 2019. Low-cost fluoride adsorbents prepared from a renewable biowaste: syntheses, characterization and modeling studies. *Arab. J. Chem.* 12 (8), 3004–3017. <https://doi.org/10.1016/j.arabjc.2015.06.028>.
- Sajidu, S., Kayira, C., Masamba, W., Mwatseteza, J., 2012. Defluoridation of groundwater using raw bauxite: rural domestic defluoridation technology. *Environ. Nat. Resour. Res.* 2 (3). <https://doi.org/10.5539/enrr.v2n3p1>.
- Salifu, A., Petrushevski, B., Mwampashi, E.S., Pazi, I.A., Ghebremichael, K., Buamah, R., Kenedy, M.D., 2016. Defluoridation of groundwater using aluminum-coated bauxite: optimization of synthesis process conditions and equilibrium study. *J. Environ. Manag.* 181 (2016), 108–117. <https://doi.org/10.1016/j.jenvman.2016.06.011>.
- Sharma, P.K., Sohail, A., Bishnu, K.S., 2021. Cost and feasibility analysis of chromium removal from water using agro and horticultural wastes as adsorbents. *RILEM Bookseries* 29, 449–463.
- Singh, P.K., Saharan, V.K., George, S., 2018. Studies on performance characteristics of calcium and magnesium amended alumina for defluoridation of drinking water. *J.*

- Environ. Chem. Eng. 6 (1), 1364–1377. <https://doi.org/10.1016/j.jece.2018.01.053>.
- Sivarajasekar, N., Paramasivan, T., Muthusaravanan, S., Muthukumar, P., Sivamani, S., 2017. Defluoridation of water using adsorbents-A concise review A BSTRAC. Journal of Environment and Biotechnology Research 6 (1), 186–198. Retrieved from [www.vinanie.com/jebr](http://www.vinanie.com/jebr).
- Sujana, M.G., Anand, S., 2011. Fluoride removal studies from contaminated ground water by using bauxite. Desalination 267 (2–3), 222–227. <https://doi.org/10.1016/j.desal.2010.09.030>.
- Sundaram, C.S., Viswanathan, N., Meenakshi, S., 2008. Uptake of fluoride by nano-hydroxyapatite/chitosan, a bioinorganic composite. Bioresour. Technol. 99 (17), 8226–8230. <https://doi.org/10.1016/j.biortech.2008.03.012>.
- Suneetha, M., Sundar, B.S., Ravindhranath, K., 2014. Studies on fluoride removal from polluted waters using active carbon derived from stems of *Abutilon indicum* plant. J. Chem. Pharmaceut. Res. 6 (10), 574–592.
- TBS, 2009. National Environmental Standards Compendium.
- Thole, B., Masamba, W.R.L., Mtaló, F.W., 2013. Water defluoridation by bauxite-gypsum magnesite (B-G-Mc) based filters calcined at 350 - 500 °C. Int. J. Phys. Sci. 8 (19), 956–962. <https://doi.org/10.5897/ijps10.668>.
- Thole, B., Mtaló, F., Masamba, W., 2012a. Effect of particle size on loading capacity and water quality in water defluoridation with 200 °C calcined bauxite, gypsum, magnesite and their composite filter. Afr. J. Pure Appl. Chem. 6 (2), 26–34. <https://doi.org/10.5897/AJPAC11.037>.
- Thole, B., Mtaló, F., Masamba, W., 2012b. Groundwater defluoridation with raw bauxite, gypsum, magnesite, and their composites. Clean 40 (11), 1222–1228. <https://doi.org/10.1002/clen.201100111>.
- Tirkey, P., Tanushree, B., Sukalyan, C., 2018. Optimization of fluoride removal from aqueous solution using jamun (*syzygium cumini*) leaf ash. Process Saf. Environ. Protect. 115, 125–138.
- USGS, 2020. Mineral Commodity Summaries 2020, United States Geological Survey, pp. 1–184. Retrieved from <https://pubs.usgs.gov/periodicals/mcs2020/mcs2020.pdf>.
- USGS, 2021. Mineral Commodity Summaries 2021. United States Geological Survey, pp. 1–199.
- Viswanathan, G., Gopalakrishnan, S., Siva Ilango, S., 2010. Assessment of water contribution on total fluoride intake of various age groups of people in fluoride endemic and non-endemic areas of Dindigul District, Tamil Nadu, South India. Water Res. 44 (20), 6186–6200. <https://doi.org/10.1016/j.watres.2010.07.041>.
- Viswanathan, N., Sundaram, C.S., Meenakshi, S., 2009. Sorption behaviour of fluoride on carboxylated cross-linked chitosan beads. Colloids Surf. B Biointerfaces 68 (1), 48–54. <https://doi.org/10.1016/j.colsurfb.2008.09.009>.
- Viswanathan, N., Meenakshi, S., 2008a. Enhanced fluoride sorption using La(III) incorporated carboxylated chitosan beads. J. Colloid Interface Sci. 322 (2), 375–383. <https://doi.org/10.1016/j.jcis.2008.03.007>.
- Viswanathan, N., Meenakshi, S., 2008b. Selective sorption of fluoride using Fe(III) loaded carboxylated chitosan beads. J. Fluor. Chem. 129 (6), 503–509. <https://doi.org/10.1016/j.jfluchem.2008.03.005>.
- Viswanathan, N., Meenakshi, S., 2009. Role of metal ion incorporation in ion exchange resin on the selectivity of fluoride. J. Hazard Mater. 162 (2–3), 920–930. <https://doi.org/10.1016/j.jhazmat.2008.05.118>.
- Wasana, H.M.S., Perera, G.D.R.K., De Gunawardena, P.S., Bandara, J., 2015. The impact of aluminum, fluoride, and aluminum-fluoride complexes in drinking water on chronic kidney disease. Environ. Sci. Pollut. Control Ser. 22 (14), 11001–11009. <https://doi.org/10.1007/s11356-015-4324-y>.
- WHO, 2011. Guidelines for Drinking-Water Quality, fourth ed. World Health Organization, pp. 1–541. [https://doi.org/10.1016/S1462-0758\(00\)00006-6](https://doi.org/10.1016/S1462-0758(00)00006-6).
- Zhao, X., Zhang, L., Xiong, P., Ma, W., Qian, N., Lu, W., 2015. A novel method for synthesis of Co-Al layered double hydroxides and their conversions to mesoporous CoAl<sub>2</sub>O<sub>4</sub> nanostructures for applications in adsorption removal of fluoride ions. Microporous Mesoporous Mater. 201 (C), 91–98. <https://doi.org/10.1016/j.micromeso.2014.09.030>.